IEEE Journal of Microwaves

Received 4 October 2022; revised 9 December 2022 and 9 December 2022; accepted 9 December 2022.
Date of current version 6 January 2023.

Digital Object Identifier 10.1109/JMW.2022.3228724

A Tutorial on the Sequential Sampling Impulse Radar Concept and Selected Applications

MARTIN VOSSIEK (Fellow, IEEE), NIKLAS HABERBERGER, LENA KRABBE (Student Member, IEEE), MARKUS HEHN (Member, IEEE), CHRISTIAN CARLOWITZ (Member, IEEE), AND MICHAEL STELZIG

(Invited Paper)

Institute of Microwaves and Photonics, Friedrich-Alexander-Universität Erlangen-Nürnberg, 91058 Erlangen, Germany

CORRESPONDING AUTHOR: Martin Vossiek (e-mail: martin.vossiek@fau.de).

This work was supported in part by the German Space Agency at DLR funded by the German Federal Ministry for Economic Affairs and Climate Action (BMWK) through Project TRIPLE-FRS under Grant 50RK2050; in part by the Elite Network of Bavaria, funded by the Bavarian State Ministry of Science and the Arts through Project IDK M^3OCCA; and in part by the Deutsche Forschungsgemeinschaft (DFG; German Research Foundation; SFB 1483) under Project 442419336, EmpkinS.
This work did not involve human subjects or animals in its research.

ABSTRACT The sequential sampling impulse radar is a radar concept that has been known for a very long time. Ultrawideband (UWB) radar systems have been realized based on this concept long before the popular phrases UWB and UWB radar were created. Its hardware simplicity, low cost, potentially high bandwidth and high range resolution, as well as the unsurpassed low power consumption of some of its variants have made it one of the most widely used radar concepts in industrial automation today. Despite its widespread use in practice, however, there are only few publications, textbooks and tutorials that describe this concept in detail and all its varieties and aspects. Especially, the correlation properties and the resulting signal-to-noise ratio (SNR), as well as the phase injection locking of pulsed oscillators, that is required for power-efficient options, have rarely been described in detail. This tutorial introduces the typical sequential sampling impulse radar concept step by step and presents the characteristics and pros and cons. As for the correlation properties and the SNR, the concepts are compared to those of standard coherent impulse radar systems and of frequency modulated continuous wave (FMCW) radar. In addition to the system theory, selected applications are presented to illustrate the attractiveness and elegance, but also the limits, of this interesting and important radar concept. The shown applications range from those in the main field of use of this type of radar, that is, industrial automation, to former and current radar concepts in the areas of automotive radar, ground penetrating radar (GPR), security scanners, and biomedical radar systems.

INDEX TERMS Automotive radar, correlation receiver, ground penetrating radar, impulse radar, MTT 70th Anniversary Special Issue, level radar, security scanner, sequential sampling, switched oscillator, system theory.

I. INTRODUCTION

Since the invention of radar technology in the early 1900s, many types of radar systems have been developed. One of the most common ways of classifying these different systems is to divide them into time domain and frequency domain radar systems. Time domain radar systems typically use a short impulse as measurement signal and are called impulse radar. Frequency domain radar systems use frequency modulated signals, such as frequency shift keying (FSK), frequency modulated continuous wave (FMCW) or orthogonal frequency division multiplexing (OFDM) signals. In a frequency domain radar, a transform from frequency domain to time domain, such as by a Fourier transform, is needed to obtain the impulse response and the time delay of the echoes of the respective targets.

Both radar variants have advantages and disadvantages. In commercial applications, such as automotive radar, frequency domain radars such as continuous wave (CW) radar systems dominate today because they provide a better signal-to-noise ratio (SNR), a higher dynamic range, and very

advantageous options for velocity measurements. The digital baseband system and signal processing are much simpler and less expensive for a CW radar than for powerful modern impulse radar systems with impulse-compressing correlation receivers. However, in applications with large target distances, the phase noise limits the applicability of CW radar systems [1], [2]. Thus, the impulse radar concept is the standard option in military, aerial, or sea surveillance, as well as remote sensing radar systems.

However, an impulse radar can also offer decisive advantages in commercial short- and medium-range applications. Some of their variants can be realized with very low-cost and compact hardware. Other impulse radar implementations can be designed to consume significantly less power than CW radar systems. Both properties are interesting for applications in industry, in building technology, or for handheld or mobile radar systems, or whenever low weight and low cost are important. This paper focuses on these commercial short- and medium-range impulse radar applications. It will show that both of the previously mentioned potential advantageous properties of impulse radar systems are significantly based on the principle of sequential sampling. Despite the long-time use of the sequential sampling radar principle, only few publications, textbooks, and tutorials describe it in detail and in all its varieties and aspects. Thus, this tutorial explains in detail the sequential sampling impulse radar concept and its characteristics.

This paper is structured as follows. Section II gives a brief overview of the functionality of a standard coherent impulse Doppler radar system. The illustrations in this section define important terms and explain the central challenges and benchmarks in impulse radar systems. Section II briefly introduces the basic principle of sequential sampling. Section III gives insights into different realization options and the signal model behind sequential sampling impulse radar systems. Section IV describes the principle and the underlying theory of impulse radar systems with switched oscillators. Section V shows several selected application examples. Finally, Section VI compares different radar principles to conclude this paper.

Notation: Underscore denotes a complex number; * the conjugate of a complex number; $|\cdot|$ the absolute value of a complex number; $*$ the convolution operator; $\mathcal{F}\{\cdot\}$ the Fourier transform operator; and env$\{\cdot\}$ the envelope operator.

II. FUNDAMENTALS

This tutorial begins with the introduction of the standard coherent impulse Doppler radar and its system theory. This will serve as a reference and benchmark for the sequential sampling impulse radar concepts that will be presented later. In addition, a brief explanation of the sequential sampling principle is given.

A. STANDARD COHERENT IMPULSE DOPPLER RADAR

A traditional impulse radar is capable only of directly measuring the distance to one or multiple targets. Hence, the target velocity v has to be estimated from the range difference between multiple measurements. This drawback can be overcome by utilizing a coherent impulse Doppler radar as shown in Fig. 1 and as explained in the following [3]. The transmit (TX) signal of the radar system s_{TX}, with the amplitude A_{TX}, the carrier frequency ω_{c}, and the transmit phase φ_{TX}, can be described as

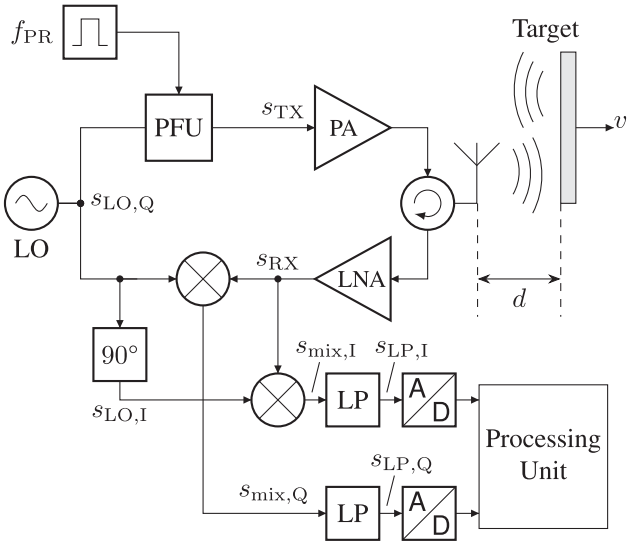

FIGURE 1. Block diagram of a coherent impulse Doppler radar, with local oscillator (LO), pulse-forming unit (PFU), power amplifier (PA), low noise amplifier (LNA), lowpass (LP) filter, and analog-to-digital (A/D) converter.

$$s_{\mathrm{TX}}(t) = A_{\mathrm{TX}} \cdot g(t) \cdot \cos\left(\omega_{\mathrm{c}} t + \varphi_{\mathrm{TX}}\right). \tag{1}$$

Here, $g(t)$ denotes the shape of the output pulse that is generated by a pulse former unit (PFU) in the TX path. In the illustration of this paper, $g(t)$ is assumed to be Gaussian. The PFU typically consists of a switch that is closed for a short time, an amplifier that is switched on during the pulse period, or a mixer, which upconverts a baseband impulse with a local oscillator (LO). Other impulse generators are also usable as long as phase coherence between transmitter and receiver can be guaranteed. The transmit signal may be amplified by a power amplifier (PA), emitted by the antenna, and reflected by a target at a distance d moving with a velocity v. Hence, the received (RX) signal s_{RX} can be described as a time-delayed version of s_{TX} according to

$$s_{\mathrm{RX}}(t) = A_{\mathrm{RX}} \cdot g(t-\tau) \cdot \cos\left(\omega_{\mathrm{c}}(t-\tau) - \omega_{\mathrm{D}}(t-\tau/2) + \varphi_{\mathrm{RX}}\right), \tag{2}$$

with the two-way travel time τ, the Doppler frequency ω_{D} and the receive amplitude A_{RX}. The latter combines the effects of amplification, reflection strength, and propagation losses along the signal path. The receive phase φ_{RX} is typically a combination of φ_{TX} and the potential phase shift due to the reflection at the target. As the impulse duration τ_{p} is extremely short compared to a period of the Doppler frequency, $\omega_{\mathrm{D}}(t-\tau/2)$ is regarded as constant during a single impulse. This is at least valid for ultra-broadband and medium-range

impulse radar systems. Hence, this additional phase contribution can be added to φ_{RX} to form φ'_{RX}. The received signal is downconverted by the LO signal

$$\underline{s}_{\mathrm{LO}}(t) = A_{\mathrm{LO}} \cdot \mathrm{e}^{-\mathrm{j}(\omega_{\mathrm{c}} t + \varphi_{\mathrm{LO}})}, \tag{3}$$

with the amplitude A_{LO} and the constant phase term φ_{LO}. With the in-phase and quadrature (IQ) mixer, we obtain the signal after the lowpass filter as

$$\begin{aligned}\underline{s}_{\mathrm{LP}}(t) &= s_{\mathrm{LP,I}}(t) + \mathrm{j}s_{\mathrm{LP,Q}}(t)\\ &= \mathrm{LP}\left\{\underline{s}_{\mathrm{LO}}(t) \cdot s_{\mathrm{RX}}(t)\right\}\\ &= \mathrm{LP}\left\{A_{\mathrm{RX}} \cdot A_{\mathrm{LO}} \cdot \mathrm{e}^{-\mathrm{j}(\omega_{\mathrm{c}} t + \varphi_{\mathrm{LO}})} \cdot g(t-\tau)\right.\\ &\quad \left. \cdot \frac{1}{2}\left(\mathrm{e}^{\mathrm{j}(\omega_{\mathrm{c}}(t-\tau) + \varphi'_{\mathrm{RX}})} + \mathrm{e}^{\mathrm{j}(-\omega_{\mathrm{c}}(t-\tau) - \varphi'_{\mathrm{RX}})}\right)\right\}\\ &= A_{\mathrm{mix}} \cdot g(t-\tau) \cdot \frac{1}{2}\mathrm{e}^{\mathrm{j}(-\omega_{\mathrm{c}}\tau + \Delta\varphi')},\end{aligned} \tag{4}$$

with $\Delta\varphi' = \varphi'_{\mathrm{RX}} - \varphi_{\mathrm{LO}}$ and $A_{\mathrm{mix}} = \frac{A_{\mathrm{LO}} A_{\mathrm{RX}}}{2}$. Through lowpass filtering, the signal components at $2\omega_{\mathrm{c}}$ are removed. Note that the IQ mixer is mandatory, as the real part of $\underline{s}_{\mathrm{LP}}(t)$ equals zero for certain combinations of $\omega_{\mathrm{c}}\tau$ and $\Delta\varphi'$. Hence, the signal amplitude of a stationary target at the corresponding distance would also be zero, which would make the target invisible to the radar system [4, S.17.2].

For further processing, $\underline{s}_{\mathrm{LP}}$ must be sampled according to the Nyquist-Shannon sampling theorem with the sampling frequency

$$f_{\mathrm{s}} \geq 2\Delta f_{\mathrm{p}} \approx \frac{2}{\tau_{\mathrm{p}}}, \tag{5}$$

with Δf_{p} as the bandwidth of the baseband impulse and τ_{p} as the impulse duration [5]. The range resolution

$$\delta_{\mathrm{R}} = \frac{c}{2\Delta f_{\mathrm{p}}} \tag{6}$$

can be described as the ability to separate two targets closely spaced in distance and as dependent on the signal bandwidth. This is because two targets can be separated only if the respective travel time difference $\Delta\tau$ is larger than τ_{p}, which is inversely proportional to the bandwidth, as already indicated in (5). For a resolution of, for example 1 m, an impulse with a bandwidth of at least 150 MHz is necessary and thus, a baseband sampling rate of more than 300 MHz is required. The requirements for the baseband system are even higher for ultrawideband (UWB) systems or short-range radar systems with resolutions below 10 cm as sampling rates of over 3 GHz are necessary. In both cases, analog-to-digital converters (ADCs) with a high sampling frequency must be used, but they have high cost, high power consumption, and a limited dynamic range.

Even if the transmit impulse duration is in the lower ns range, the LO and the ADC must still be operated until the reflection from the most distant target, and hence, from the maximum measurement range of the radar, could be received. Thus, the power consumption of a coherent impulse Doppler radar is typically not lower than of a CW radar. Furthermore, the short impulse duration used in an impulse Doppler radar inherently yields a poor SNR as can be calculated by

$$\mathrm{SNR} = \frac{|A_{\mathrm{RX}}|^2}{N^2} \int_{t=0}^{\tau_{\mathrm{p}}} |g(t)|^2 \, \mathrm{d}t, \tag{7}$$

with the noise power N. This can also be explained by the comparably small average transmitted power P_{avg} of such a radar system, which is described by

$$P_{\mathrm{avg}} = P_{\mathrm{peak}} \cdot \tau_{\mathrm{p}} \cdot f_{\mathrm{PR}}. \tag{8}$$

Due to technical challenges and legal regulations, the peak output power P_{peak} is limited [4, S.1.3]. Moreover, increasing the pulse repetition frequency (PRF) f_{PR} leads to a decreasing maximum unambiguous range according to

$$d_{\mathrm{max}} = \frac{c}{2 \cdot f_{\mathrm{PR}}}. \tag{9}$$

As a consequence, an application-specific compromise must be found between range resolution, unambiguous range, and achievable SNR.

By integrating multiple pulses, it is possible to increase the SNR depending on the dwell time in which the target resides in the main antenna beam. Without averaging, the use of pulse compression techniques can help overcome the limitations posed by the compromise between a high resolution and a high range or SNR. To achieve this, longer signals with good self-correlation properties e.g. chirps, Barker-codes, or M-sequences are transmitted. A correlation receiver is used to compress these signals to a short impulse. The maximum SNR is achieved with a matched filter with the impulse response

$$\underline{h}_{\mathrm{RX,opt}}(t) = \gamma \cdot \underline{s}^*(-t), \tag{10}$$

which is the time-inverse complex conjugate of the transmit signal $\underline{s}(t)$ multiplied by an arbitrary constant γ. Hereby, the transmitted average power is drastically enlarged, while a high range resolution is still maintained. The maximum SNR enhancement k using correlation can be derived from the time-bandwidth-product as

$$k = \Delta f_{\mathrm{p}} \cdot \tau_{\mathrm{p}}. \tag{11}$$

If an impulse radar system utilizes pulse compression, such as with a 150 MHz bandwidth spread over a 10 μs impulse, the respective SNR can be enlarged by a factor of up to 1,500 or 31.8 dB. The filters used for such a compression are typically realized in software, but there are also possibilities in hardware, such as surface acoustic wave (SAW) filters. A drawback of lengthening the transmit signal is the possible saturation of the receiver during the transmission. Thus, a pulse compression radar can also suffer from the inability to detect targets close to the antennas [4, S.19.17].

However, impulse radar systems are increasingly being replaced by continuous wave radar systems, especially for high-performance short- and medium-range systems with high range resolution. With those high demands, the complexity of the ADC and the digital baseband processing is very

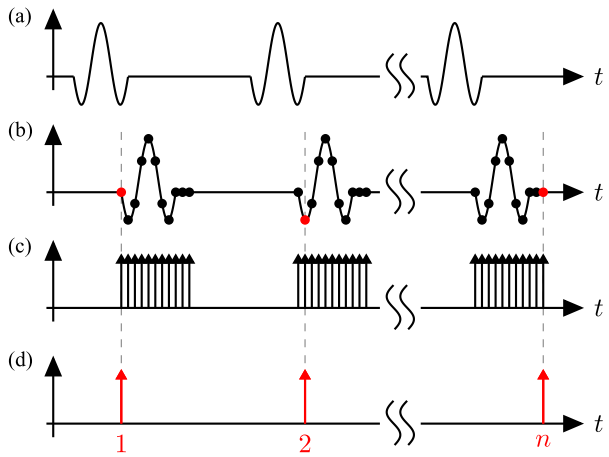

FIGURE 2. Principle of sequential sampling in contrast to real-time sampling. (a) Transmitted radar signal, (b) received radar echo, (c) real-time sampling, (d) sequential sampling.

high for the coherent impulse Doppler radar. Furthermore, the permanent usage of the LO for coherency further decreases the efficiency, which makes these systems comparably expensive to build and to operate. As will be explained later in this paper, sequential sampling radar variants can solve these drawbacks in an elegant way.

B. SEQUENTIAL SAMPLING PRINCIPLE

The sequential sampling technique was first introduced by Janssen in the early 1950s [7], [8] and was developed for commercial use by Hewlett-Packard in 1960 with the HP185A sampling oscilloscope [9]. While real-time sampling continuously observes the signal waveform, sequential sampling acquires only one sample per signal period. This is accomplished by shifting the sampling point by a small time increment from period to period, as shown in Fig. 2.

This sampling principle can be applied to radar systems when the observed scene can be regarded as static or quasi-static during the acquisition and thus, generates a periodic radar echo signal, as shown in Fig. 2(b). Accordingly, the ADC sampling frequency can be reduced compared to a standard impulse radar and is typically in the order of several hundreds of kHz [10], which can be accomplished with low-cost ADCs. As a consequence of the reduced sampling frequency, it is possible to reduce the overall system power consumption and the component costs, which makes sequential sampling a perfect choice for applications with limited production expenses [10], low battery capacity or increasing numbers of included sensors.

III. SEQUENTIAL SAMPLING IMPULSE RADAR

Section III-A presents the signal model of the sequential sampling impulse radar. Section III-B gives insights into the implementation options for several key components of the system. Relevant system properties are outlined in Section III-C, and Section III-D introduces a common method of SNR improvement.

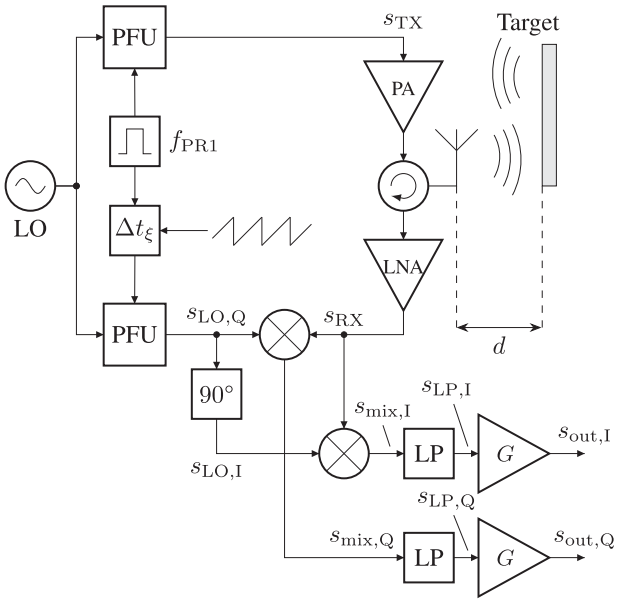

FIGURE 3. Radar system block diagram with an adjustable delay element to generate a delayed local oscillator (LO) signal. With pulse-forming unit (PFU), power amplifier (PA), low noise amplifier (LNA), lowpass (LP) filter and amplifier (G).

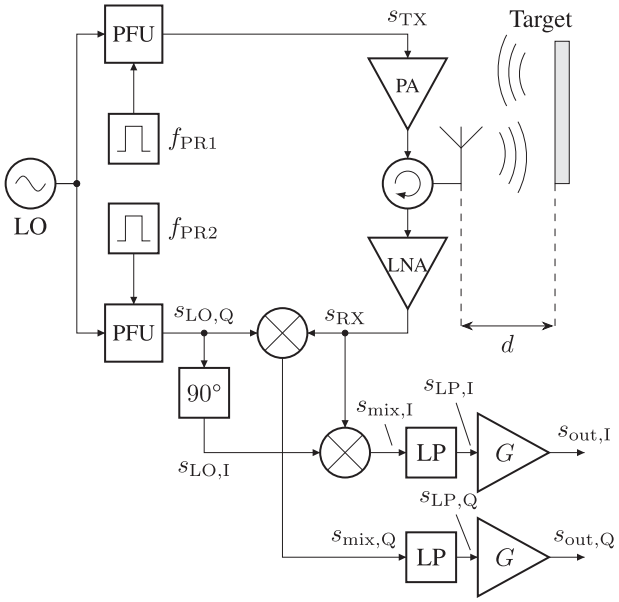

FIGURE 4. Radar system block diagram with multirate approach to generate a delayed local oscillator (LO) signal. With pulse forming unit (PFU), power amplifier (PA), low noise amplifier (LNA), low pass (LP) filter and amplifier (G).

A. SIGNAL MODEL

In this section, a general signal model of a sequential sampling pulse radar is derived, based on its simplified block diagram shown in Figs. 3 and 4. Those figures differ in the implementation of the sequential sampling procedure itself, which is discussed in Section III-B. Additionally, the relevant signals of the observed sequential sampling system are outlined

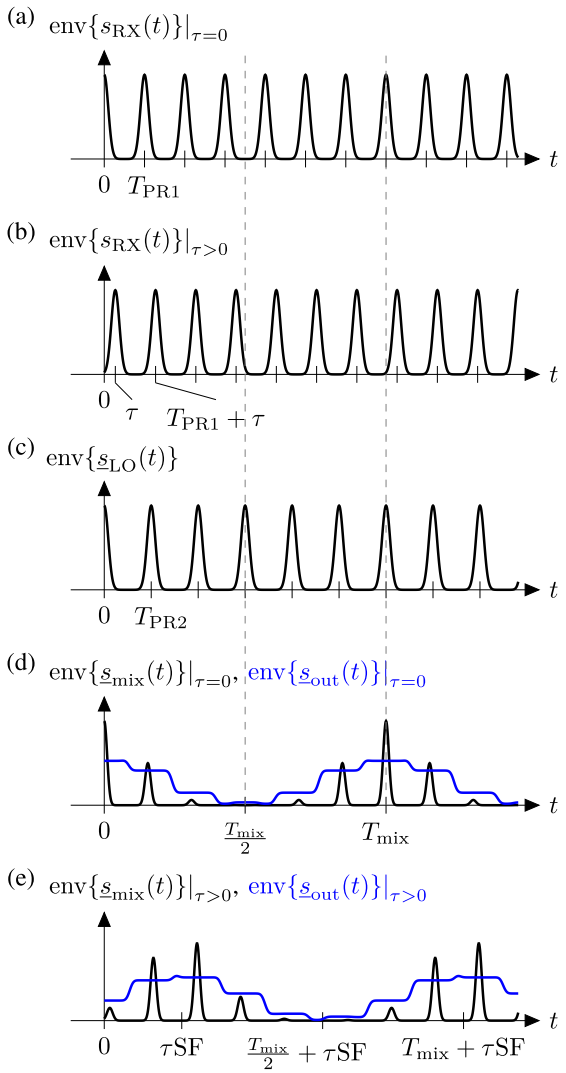

FIGURE 5. Envelope of sample signals in the process chain of a sequential sampling radar: (a) received signal for $\tau = 0$, (b) received signal for $\tau > 0$, (c) LO-signal, (d) mixer output signal (black) and final output signal (blue) for $\tau = 0$, and (e) mixer output signal (black) and final output signal (blue) for $\tau > 0$.

schematically in Fig. 5 to illustrate the functionalities of the different system components. The variables used in Section II will not be introduced again.

The transmitted signal $s_{\mathrm{TX}}(t)$ consists of a series of pulses with a PRF f_{PR1} given by

$$f_{\mathrm{PR1}} = \frac{1}{T_{\mathrm{PR1}}}. \tag{12}$$

This sequence of pulses can be described as

$$p_{\mathrm{TX}}(t) = g(t) * \mathrm{III}_{T_{\mathrm{PR1}}}(t) = \sum_{\mu=-\infty}^{\infty} g(t - \mu T_{\mathrm{PR1}}), \tag{13}$$

incorporating $\mathrm{III}_{T_{\mathrm{PR1}}}(t)$ as a pulse train with a pulse-to-pulse interval of T_{PR1}. The resulting signal $s_{\mathrm{TX}}(t)$ given by

$$s_{\mathrm{TX}}(t) = A_{\mathrm{TX}} \cdot p_{\mathrm{TX}}(t) \cdot \cos\left(\omega_{\mathrm{c}} t + \varphi_{\mathrm{TX}}\right) \tag{14}$$

is amplified using a PA and transmitted by the antenna. When the transmitted signal is reflected by a target at a distance d, the antenna detects the echo signal

$$s_{\mathrm{RX}}(t) = A_{\mathrm{RX}} \cdot p_{\mathrm{RX}}(t) \cdot \cos\left(\omega_{\mathrm{c}}(t - \tau) + \varphi_{\mathrm{RX}}\right), \tag{15}$$

which is visualized in Fig. 5(b). The pulse train of the received echo signal is given by

$$p_{\mathrm{RX}}(t) = g(t - \tau) * \mathrm{III}_{T_{\mathrm{PR1}}}(t) = p_{\mathrm{TX}}(t - \tau). \tag{16}$$

Thereafter, the received and amplified echo signal $s_{\mathrm{RX}}(t)$ is demodulated using an IQ mixer. This mixing operation corresponds to the multiplication of $s_{\mathrm{RX}}(t)$ with the complex LO signal $\underline{s}_{\mathrm{LO}}(t)$, which yields

$$\underline{s}_{\mathrm{mix}}(t) = s_{\mathrm{RX}}(t) \cdot \underline{s}_{\mathrm{LO}}(t). \tag{17}$$

In contrast to the standard impulse Doppler radar described in Section II, the LO-signal $\underline{s}_{\mathrm{LO}}(t)$ used for the sequential sampling is a pulsed signal. Therefore, it can be described by

$$\begin{aligned}\underline{s}_{\mathrm{LO}}(t) &= s_{\mathrm{LO,I}}(t) + \mathrm{j}s_{\mathrm{LO,Q}}(t) \\ &= A_{\mathrm{LO}} \cdot p_{\mathrm{LO}}(t) \cdot \mathrm{e}^{-\mathrm{j}(\omega_{\mathrm{c}} t + \varphi_{\mathrm{LO}})},\end{aligned} \tag{18}$$

with the pulse train $p_{\mathrm{LO}}(t)$ according to

$$\begin{aligned}p_{\mathrm{LO}}(t) = g(t) * \mathrm{III}_{T_{\mathrm{PR2}}}(t) &= \sum_{\nu=-\infty}^{\infty} g(t - \nu T_{\mathrm{PR2}}) \\ &= \sum_{\nu=-\infty}^{\infty} g\left(t - \left(\nu T_{\mathrm{PR1}} + \Delta t_{\xi}\right)\right).\end{aligned} \tag{19}$$

Note that in an ideal implementation φ_{TX}, would be equal to φ_{LO}. However, in a real setup, the phase terms of the TX and LO paths are different but usually constant because of, for example, unequal transmission line lengths.

The pulse train $p_{\mathrm{LO}}(t)$ has a slightly different pulse-to-pulse interval $T_{\mathrm{PR2}} > T_{\mathrm{PR1}}$ to generate a small time increment ΔT_{PR} from period to period, as shown in Fig. 2. In relation to the global time t, the time increment can be written as $\Delta t_{\xi} = \xi(\nu) \cdot \Delta T_{\mathrm{PR}}$ and can usually be simplified to

$$\Delta t_{\xi} = \nu \cdot \Delta T_{\mathrm{PR}}. \tag{20}$$

This time increment corresponds to a slightly reduced PRF f_{PR2}, given by

$$f_{\mathrm{PR2}} = \frac{1}{T_{\mathrm{PR2}}} = f_{\mathrm{PR1}} - \Delta f_{\mathrm{PR}} = \frac{1}{T_{\mathrm{PR1}} + \Delta T_{\mathrm{PR}}}. \tag{21}$$

From this, we obtain the time increment ΔT_{PR} as

$$\Delta T_{\mathrm{PR}} = T_{\mathrm{PR2}} - T_{\mathrm{PR1}} = \frac{\Delta f_{\mathrm{PR}}}{f_{\mathrm{PR1}} f_{\mathrm{PR2}}} \approx \frac{\Delta f_{\mathrm{PR}}}{f_{\mathrm{PR1}}^2}. \tag{22}$$

Accordingly, the PRF difference Δf_{PR} between the LO and the received echo signal is written as

$$\Delta f_{\mathrm{PR}} = f_{\mathrm{PR1}} - f_{\mathrm{PR2}} = \frac{\Delta T_{\mathrm{PR}}}{T_{\mathrm{PR1}} T_{\mathrm{PR2}}} \approx \frac{\Delta T_{\mathrm{PR}}}{T_{\mathrm{PR1}}^2}. \tag{23}$$

Proceeding from (17), the complex mixer output signal $\underline{s}_{\mathrm{mix}}(t)$ is lowpass-filtered to remove the undesired frequency components generated in the mixing process. Moreover, to a good approximation, this low pass filter with the cut-off frequency $f_{\mathrm{cut,LP}}$ also functions as an integrator for $f \gg f_{\mathrm{cut,LP}}$ [11]. Therefore, we obtain

$$\underline{s}_{\mathrm{LP}}(t) = \mathrm{LP}\{\underline{s}_{\mathrm{mix}}(t)\} = \frac{1}{T_{\mathrm{LP}}} \int_{t-\frac{T_{\mathrm{LP}}}{2}}^{t+\frac{T_{\mathrm{LP}}}{2}} \underline{s}_{\mathrm{mix}}(t')\,\mathrm{d}t' \tag{24}$$

after applying the low pass filter. Fig. 5(d) sketches the envelope of $\underline{s}_{\mathrm{mix}}(t)$ and $\underline{s}_{\mathrm{out}}(t)$ for the hypothetical case of $\tau = 0$, showing that $\underline{s}_{\mathrm{out}}(t)$ is a stretched version of $s_{\mathrm{TX}}(t)$ with a new pulse-to-pulse interval T_{mix} according to

$$T_{\mathrm{mix}} = \mathrm{SF} \cdot T_{\mathrm{PR1}}. \tag{25}$$

Therein, SF is the so-called spreading factor or scaling factor, which is also described by

$$\mathrm{SF} = \frac{f_{\mathrm{PR1}}}{\Delta f_{\mathrm{PR}}} = \frac{T_{\mathrm{PR2}}}{\Delta T_{\mathrm{PR}}}. \tag{26}$$

Accordingly, the integration time T_{LP} has to be designed such that the low pass filter passes each stretched pulse completely and without distortion. This is accomplished by defining the T_{LP} according to [12] as

$$T_{\mathrm{LP}} = 2\tau_{\mathrm{p}}\mathrm{SF} = 2\frac{\mathrm{SF}}{\Delta f_{\mathrm{p}}}. \tag{27}$$

As τ_{p} is defined as the 3 dB pulse width, an additional factor 2 arises in (27) to cover the complete pulse. As a consequence of stretching in time, the cut-off frequency $f_{\mathrm{cut,LP}}$ of the low pass filter can be approximated as the compressed pulse bandwidth according to

$$f_{\mathrm{cut,LP}} \approx \frac{\Delta f_{\mathrm{p}}}{\mathrm{SF}}. \tag{28}$$

As a last step, the lowpass-filtered signal $\underline{s}_{\mathrm{LP}}(t)$ is amplified, yielding

$$\underline{s}_{\mathrm{out}}(t) = G \cdot \underline{s}_{\mathrm{LP}}(t). \tag{29}$$

Fig. 5(e) sketches the signals $\underline{s}_{\mathrm{mix}}(t)$ and $\underline{s}_{\mathrm{out}}(t)$ for a target located at distance $d > 0$. Therein, the peak in $\underline{s}_{\mathrm{out}}(t)$ is shifted by $\tau\,\mathrm{SF}$ and can be used to estimate the distance of the target. Due to the stretching effect in the time domain, the output signal shows an effective sampling rate of

$$f_{\mathrm{s,eff}} = \mathrm{SF} \cdot f_{\mathrm{PR2}} = \frac{f_{\mathrm{PR1}} f_{\mathrm{PR2}}}{\Delta f_{\mathrm{PR}}} = \frac{1}{\Delta T_{\mathrm{PR}}}. \tag{30}$$

Accordingly, the actual sampling rate can be reduced by exactly the spreading factor SF, while the Nyquist-Shannon sampling theorem from (5) must still be satisfied. For example, with a PRF of $f_{\mathrm{PR2}} = 1\,\mathrm{MHz}$ and a spreading factor of $\mathrm{SF} = 10{,}000$, the effective sampling rate would be $f_{\mathrm{s,eff}} = 10\,\mathrm{GHz}$, which means that signals with a maximum of 5 GHz can be sampled while complying with the Nyquist–Shannon criteria.

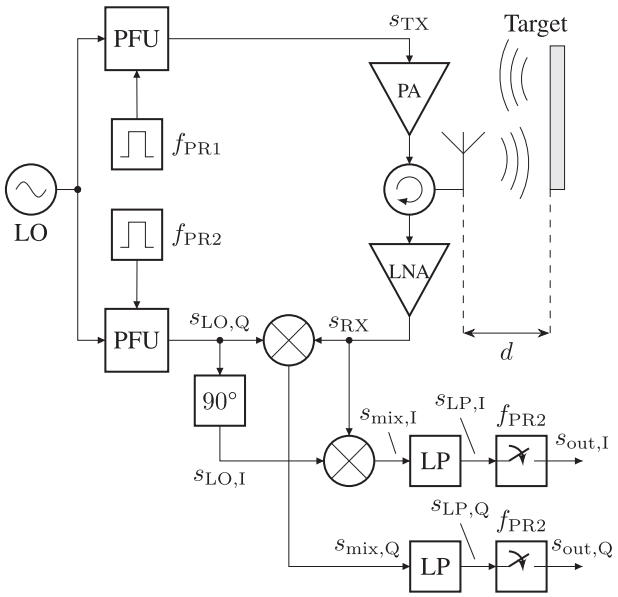

FIGURE 6. Implementation of a sequential sampling radar with sample-and-hold (S&H) circuit and multirate approach. With local oscillator (LO), pulse forming unit (PFU), power amplifier (PA), low noise amplifier (LNA) and low pass (LP) filter.

B. IMPLEMENTATION OPTIONS

In this section, we examine different implementation options for the generation of the time shift Δt_ξ and for the processing of the mixer output signal $\underline{s}_{\mathrm{mix}}(t)$.

1) SHIFT GENERATION

To sequentially sample the received radar echo, the generation of the time shift Δt_ξ between the transmitted signal $s_{\mathrm{TX}}(t)$ and the LO-signal $\underline{s}_{\mathrm{LO}}(t)$ is an essential system component. Two basic implementation options will be explained next.

One option for realizing the delay Δt_ξ is to include an adjustable delay element in the LO-path, as shown in Fig. 3 [13]. As shown in (20), the delay increases with the increasing number of transmitted pulses. This can be realized with a suitable saw-tooth signal, as suggested in [14].

Another option is the widely used multirate approach [15], [16], [17]. Therein, two different PRFs are used to generate the time shift Δt_ξ, usually with a smaller f_{PR2} in the LO-path. The corresponding block diagram is shown in Fig. 4.

2) MIXER OUTPUT PROCESSING

One option for processing the mixer output signal $\underline{s}_{\mathrm{mix}}(t)$ has been described in the signal model in the previous section and is illustrated, for example in Fig. 4. This option includes a narrow-band low pass filter, causing the signal energy of the narrow pulses to be spread in time according to (27). As a result, the amplitude of the low pass filter output signal $\underline{s}_{\mathrm{LP}}(t)$ is reduced significantly. Therefore, an amplifier with high gain is needed to enable further processing, as it is described in the signal model. Sample signals for the amplified output signal $\underline{s}_{\mathrm{out}}(t)$ can be seen in blue in Fig. 5(d) and 5(e). However,

the amplifier also introduces more noise into the signal chain, which reduces the overall performance of this implementation option.

Another processing option is to use a fast sample-and-hold (S&H) element [4, S.19.20] which is illustrated in Fig. 6. Therein, the used low pass filter can be designed in such a way that it only suppresses the unwanted frequency component at $2\omega_c$, which results from the mixing process. Therefore, the signal energy is not spread by the low pass filter and thus, a high gain amplifier is not necessary compared to the implementation method described before. However, the implementation option with an S&H element is not widely used, as suitable S&H elements with good properties are expensive, and in most cases, building them is not reasonable.

C. SYSTEM PROPERTIES

This section covers the following relevant system properties: correlation characteristics, noise bandwidth, and SNR.

1) CORRELATION CHARACTERISTICS

When looking only at a single pulse, for example, with $\mu = \nu = 0$ and arbitrary ξ, we can calculate the output signal $\underline{s}_{\text{out}}(t)$ as

$$\begin{aligned}\underline{s}_{\text{out}}(t) &= \frac{G}{T_{\text{LP}}}\int_{t-\frac{T_{\text{LP}}}{2}}^{t+\frac{T_{\text{LP}}}{2}} s_{\text{RX}}(t')\cdot \underline{s}_{\text{LO}}(t')\,\mathrm{d}t' \\ &\overset{\text{(a)}}{=} \frac{G'A'}{T_{\text{LP}}}\mathrm{e}^{\mathrm{j}(-\omega_c\tau+\Delta\varphi)}\int_{t-\frac{T_{\text{LP}}}{2}}^{t+\frac{T_{\text{LP}}}{2}} g(t'-\tau)g\left(t'-\Delta t_\xi\right)\,\mathrm{d}t' \\ &\overset{\text{(b)}}{\approx} \frac{G'A'}{T_{\text{LP}}}\mathrm{e}^{\mathrm{j}(-\omega_c\tau+\Delta\varphi)}\int_{-\infty}^{\infty} g(\tau')g(\tau'+\Delta t_\xi-\tau)\,\mathrm{d}\tau' \\ &\overset{\text{(c)}}{=} \frac{G'A'}{T_{\text{LP}}}\mathrm{e}^{\mathrm{j}(-\omega_c\tau+\Delta\varphi)}\Psi_{gg}\left(\Delta t_\xi-\tau\right), \end{aligned} \tag{31}$$

where $\Delta\varphi = \varphi_{\text{RX}} - \varphi_{\text{LO}}$, $G' = GG_{\text{LNA}}$ and $A' = \frac{A_{\text{LO}}A_{\text{RX}}}{2}$. In step (a), the frequency component around $2\omega_c$ resulting from the mixing process was eliminated, as this component is removed by the low pass filter. Furthermore, in step (b) we substitute τ' according to $\tau' = t' - \Delta t_\xi$ and change the integration limits accordingly. The latter is possible because $\tau_p \ll T_{\text{LP}} = 2\tau_p\text{SF}$ is valid for applications with high values of SF. Finally, in step (c), the integral is replaced by the definition of the autocorrelation function (AKF) Ψ_{gg} of the shifted basic pulse $g(\tau')$. Therefore, the low pass filter following a mixer is often labeled as an *analog correlator* [18]. The calculation in (31) shows, that the sequential sampling technique inherently provides a correlation receiver.

2) NOISE BANDWIDTH

When transforming the LO time signal $\underline{s}_{\text{LO}}(t)$ into the frequency domain, we obtain

$$\begin{aligned}\underline{S}_{\text{LO}}(f) &= \mathcal{F}\{\underline{s}_{\text{LO}}(t)\} \\ &= A_{\text{LO}}\cdot f_{\text{PR2}}\mathcal{F}\{g(t)\}\text{Ш}_{f_{\text{PR2}}}(f) * \mathrm{e}^{\mathrm{j}\varphi_{\text{LO}}}\delta(f-f_c), \end{aligned} \tag{32}$$

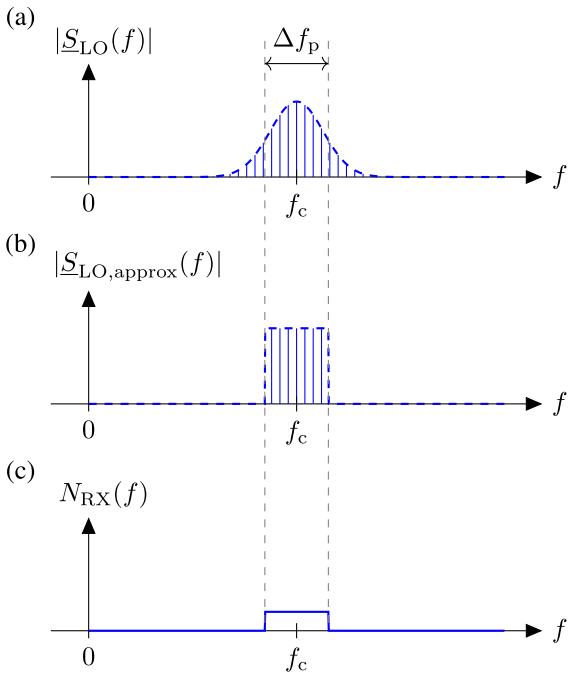

FIGURE 7. (a) Power density spectrum of the LO signal, (b) approximated power density spectrum of the LO signal, and (c) noise power density spectrum of the received signal.

which is sketched in Fig. 7(a). Because of a periodically repeating signal in time, the spectrum $\underline{S}_{\text{LO}}(f)$ is a line spectrum with a line spacing of f_{PR2}, centered at the frequency f_c. To simplify the description, we approximate $\underline{S}_{\text{LO}}(f)$ by neglecting the amplitude weights of the spectral lines and by reducing the spectrum width to Δf_p. The resulting approximation $\underline{S}_{\text{LO,approx}}(f)$ is shown in Fig. 7(b). The number of relevant spectral lines can be obtained as follows:

$$N_\ell = \frac{\Delta f_p}{f_{\text{PR2}}}. \tag{33}$$

The multiplication of two signals in the mixing process is equivalent to a convolution of the corresponding frequency spectra. Therefore, each of the N_ℓ spectral lines in $\underline{S}_{\text{LO,approx}}(f)$ converts a part of the power density spectrum $N_{\text{RX}}(f)$ of the received noise signal into the pass band of the low pass filter that follows the mixer. This noise spectrum $N_{\text{RX}}(f)$ is inherently bandpass-filtered by the antenna and the LNA with a bandwidth of Δf_p around the carrier frequency f_c. As a consequence of the mixing process, we obtain the equivalent noise bandwidth $\Delta f_{\text{n,ss}}$ at the output of the low pass filter of the sequential sampling system as

$$\Delta f_{\text{n,ss}} = N_\ell \Delta f_{\text{LP}} = \frac{\Delta f_p}{f_{\text{PR2}}}\frac{\Delta f_p}{\text{SF}} \approx \Delta f_p^2 \Delta T_{\text{PR}}, \tag{34}$$

with the low pass filter bandwidth Δf_{LP}. However, when is noise added to the signal after the mixing process, we obtain a noise bandwidth of

$$\Delta f_{\text{n,ss}} = \frac{\Delta f_p}{\text{SF}}. \tag{35}$$

Therefore, we can describe the noise bandwidth of the sequential sampling radar by introducing a lower and upper limit according to

$$\frac{\Delta f_{\mathrm{p}}}{\mathrm{SF}} \leq \Delta f_{\mathrm{n,ss}} \leq \Delta f_{\mathrm{p}}^2 \Delta T_{\mathrm{PR}}. \tag{36}$$

In contrast to the noise bandwidth $\Delta f_{\mathrm{n,p}}$ of an impulse radar system described by

$$\Delta f_{\mathrm{n,p}} = \Delta f_{\mathrm{p}} \approx \frac{1}{\tau_{\mathrm{p}}}, \tag{37}$$

the noise bandwidth $\Delta f_{\mathrm{n,ss}}$ of the sequential sampling radar system is reduced. Accordingly, we obtain a minimum reduction factor of $(\Delta f_{\mathrm{p}} \Delta T_{\mathrm{PR}})^{-1}$ and a maximum of SF. Assuming a pulse width of $\tau_p = 1$ ns, a spreading factor of SF $= 10{,}000$, and a PRF of $f_{\mathrm{PR2}} = 1$ MHz, the noise bandwidth would be in the range of

$$100\,\mathrm{kHz} \leq \Delta f_{\mathrm{n,ss}} \leq 100\,\mathrm{MHz}. \tag{38}$$

3) SNR CONSIDERATIONS

With the equivalent noise bandwidth $\Delta f_{\mathrm{n,ss}}$ of the sequential sampling radar system, the SNR can be improved in comparison to the impulse radar. As a result of (36), we obtain the $\mathrm{SNR_{ss}}$ of the sequential sampling system as

$$\mathrm{SNR_{ss}} = \mathrm{SNR_p} + 10\log_{10}\left(\frac{\Delta f_{\mathrm{n,p}}}{\Delta f_{\mathrm{n,ss}}}\right), \tag{39}$$

with $\mathrm{SNR_p}$ being the SNR of the standard impulse radar system. For the sample calculation in (38), the SNR can be improved by a minimum of 10 dB and a maximum of 40 dB.

D. SNR IMPROVEMENT WITH PSEUDO RANDOM NOISE SEQUENCES

To enable the detection of a distant target, a sufficiently high SNR of the radar transmit signal is necessary, as discussed in Section II-A. Consequently, a sequential sampling impulse radar suffers under the same drawback. On the contrary, the ability to utilize pulse compression for SNR improvement is inherently given in a sequential sampling impulse radar, as the received signal is sampled with delayed TX impulses. Together with the subsequent lowpass-filtering, this can be interpreted as a correlation. Thus, a matched filter with an optimal SNR is already implemented in the hardware. A further improvement can be realized by varying the TX impulses according to their amplitude and/or their phase. By combining multiple fully sampled pulses of such kind, it is possible to increase the SNR of the complete pulse train by a subsequent correlation. A widely used and simple method of doing this is phase modulation using pseudo random noise (PRN) sequences, which show characteristics similiar to those of random sequences [4, S.10.6 ff]. PRN sequences are often realized using M-sequences, which are random sequences of zeros and ones. Those binary values correspond to a phase change of the transmitted signal pulse of zero and 180°, respectively. When incorporating an M-sequence with N_{m} binary elements, the SNR can be further improved as follows:

$$\Delta\mathrm{SNR} = 10\log_{10}(N_{\mathrm{m}}). \tag{40}$$

However, the measurement time increases drastically.

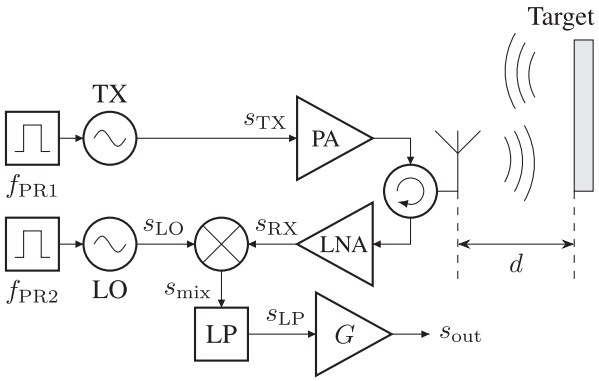

FIGURE 8. Block diagram of the sequential sampling primary radar with switched oscillators. With local oscillator in the receive path (LO) and transmit path (TX), power amplifier (PA), low noise amplifier (LNA), low pass (LP) filter and amplifier (G).

IV. IMPULSE RADAR WITH SWITCHED OSCILLATORS

This section covers a sequential sampling radar variant that is much more power-efficient and ideally suited for ultra-low-power radar systems. Section IV-A briefly introduces pulse injection locking, followed by a signal model in Chapter IV-B. Section IV-C summarizes the properties of this type of radar.

A. THEORY OF PULSE INJECTION LOCKING

As explained in the previous section, sequential sampling drastically decreases the necessary ADC sampling rate, compared to a standard impulse radar. However, it is very unsatisfactory that the LO has to run the whole time, although the carrier is used only for a few nanoseconds. Subsequently, we will take a look at a sequential sampling radar variant that is much more power-efficient and ideally suited for ultra-low-power radar systems. Instead of using one common fixed-frequency LO, from which coherent transmit and LO pulses are generated, two separate switched oscillators are utilized, as shown in Fig. 8. At first glance, one would suspect that this radar does not work, as there is actually no coherence between the phases of the transmit and receive oscillators. The averaged amplitude of the mixed signal should probably be zero, as the phase difference between the LO and TX pulses varies randomly from measurement to measurement. However, this is not the case. Contrary to what one would expect, a switched pulse oscillator usually does not start with a random phase. This behavior, called pulse injection locking, is due to the fact that the short switching pulses or non-linear processes in the oscillator itself lead to harmonics that couple into the feedback loop of the oscillator and thus, define the starting condition of the oscillation startup process [19], [20], [21], [22], [23], [24]. Since the starting condition is

identical for every switch-on cycle, a switched pulse oscillator will always start oscillating at almost the same phase. This property is not necessarily always seen in every impulse oscillator. However, with very short switching times, as they are common in impulse radar systems, this property is usually inherent in most of the common semiconductor-based RF impulse oscillator designs [23]. Nevertheless, a careful oscillator design that promotes this injection locking property can be useful for minimizing the pulse-to-pulse phase jitter. There are many publications on the design of impulse oscillators that are used in switched oscillator radar systems, for example, for the utilization in short-range automotive radar systems of around 24 GHz [25], [26]. Besides automotive radar, pulse oscillators in the same frequency range are also used in UWB systems for communication and ranging [23], [27], [28]. Even higher frequencies are realized by [29], [30], with a pulse oscillator working in the automotive long-range radar band at 79 GHz.

B. SIGNAL MODEL

In this section, the signal model of the sequential sampling radar that was introduced in Section III-A is extended using two switched oscillators. A modified block diagram of the sequential sampling radar system is shown in Fig. 8. A single oscillation $p_{\mathrm{TX}}(t)$ of the oscillator in the transmitting path can be described as follows:

$$p_{\mathrm{TX}}(t) = g_{\mathrm{TX}}(t) \cdot \cos(\omega_{\mathrm{c}} t + \varphi_{\mathrm{TX}}), \tag{41}$$

where, ω_{c} is the oscillation frequency, and φ_{TX} denotes the constant initial startup phase of the switched oscillator. Multiplied by the pulse train $\mathrm{III}_{T_{\mathrm{PR1}}}(t)$ that was introduced in (13), the resulting signal $s_{\mathrm{TX}}(t)$ is given by

$$\begin{aligned} s_{\mathrm{TX}}(t) &= A_{\mathrm{TX}} \cdot p_{\mathrm{TX}}(t) * \mathrm{III}_{T_{\mathrm{PR1}}}(t) \\ &= A_{\mathrm{TX}} \sum_{\mu=-\infty}^{\infty} p_{\mathrm{TX}}(t - \mu T_{\mathrm{PR1}}). \end{aligned} \tag{42}$$

The same applies to the LO signal $s_{\mathrm{LO}}(t)$ according to Fig. 8, yielding

$$\begin{aligned} s_{\mathrm{LO}}(t) &= A_{\mathrm{LO}} \cdot p_{\mathrm{LO}}(t) * \mathrm{III}_{T_{\mathrm{PR2}}}(t) \\ &= A_{\mathrm{LO}} \sum_{\nu=-\infty}^{\infty} p_{\mathrm{LO}}(t - \nu T_{\mathrm{PR2}}), \end{aligned} \tag{43}$$

where $p_{\mathrm{LO}}(t)$ denotes a single oscillation of the LO oscillator, described by

$$p_{\mathrm{LO}}(t) = g_{\mathrm{LO}}(t) \cdot \cos(\omega_{\mathrm{c}}' t + \varphi_{\mathrm{LO}}), \tag{44}$$

where ω_{c}' is the oscillation frequency and φ_{LO} is the initial startup phase. Due to manufacutring imperfections, the pulse shape $g_{\mathrm{LO}}(t)$, the carrier frequency ω_{c}', and the phase offset φ_{LO} can slightly differ from those of the oscillator in the TX path.

Subsequently, $s_{\mathrm{TX}}(t)$ is amplified and emitted by the antenna. The echo signal $s_{\mathrm{RX}}(t)$ can be described as follows:

$$\begin{aligned} s_{\mathrm{RX}}(t) &= A_{\mathrm{RX}} \cdot p_{\mathrm{RX}}(t) * \mathrm{III}_{T_{\mathrm{PR1}}}(t) \\ &= A_{\mathrm{RX}} \cdot \sum_{\mu=-\infty}^{\infty} p_{\mathrm{RX}}(t - \mu T_{\mathrm{PR1}}), \end{aligned} \tag{45}$$

where $p_{\mathrm{RX}}(t)$ denotes a single receive pulse, written as

$$p_{\mathrm{RX}}(t) = g_{\mathrm{TX}}(t - \tau) \cdot \cos(\omega_{\mathrm{c}}(t - \tau) + \varphi_{\mathrm{RX}}). \tag{46}$$

The mixer signal can be calculated as follows:

$$\begin{aligned} s_{\mathrm{mix}}(t) &= s_{\mathrm{RX}}(t) \cdot s_{\mathrm{LO}}(t) \\ &= A_{\mathrm{mix}} \Bigg(\sum_{\mu=-\infty}^{\infty} \sum_{\nu=-\infty}^{\infty} g_{\mathrm{TX}}(t - \tau - \mu T_{\mathrm{PR1}}) \\ &\quad \cdot g_{\mathrm{LO}}(t - \nu T_{\mathrm{PR2}}) \\ &\quad \cdot \cos\left(\omega_c \left(\nu T_{\mathrm{PR2}} - \mu T_{\mathrm{PR1}} - \tau\right) + \Delta\varphi \right. \\ &\quad \left. + \Delta\omega_{\mathrm{c}} \left(t - \nu T_{\mathrm{PR2}}\right)\right) \Bigg) + s(2\omega_{\mathrm{c}} t), \end{aligned} \tag{47}$$

with the signal amplitude $A_{\mathrm{mix}} = \frac{G_{\mathrm{LNA}} A_{\mathrm{RX}} A_{\mathrm{LO}}}{2}$, the phase difference $\Delta\varphi = \varphi_{\mathrm{RX}} - \varphi_{\mathrm{LO}}$, and the carrier frequency difference $\Delta\omega_{\mathrm{c}} = \omega_{\mathrm{c}} - \omega_{\mathrm{c}}'$. The signal components at the double carrier frequency are summarized in the signal $s(2\omega_{\mathrm{c}} t)$. (47) shows that the multiplication of two oscillator signals with a constant start-up phase and an additional increasing time shift generated by the sequential sampling results in an intermediate frequency in the mixer output signal. Therefore, only a regular mixer is necessary for demodulation of the amplified echo signal $s_{\mathrm{RX}}(t)$, which reduces the component complexity. The oscillators are only switched on for a very short time (e.g. 1 ns), and since the frequency difference $\Delta\omega_{\mathrm{c}}$ is small (e.g. 10 MHz), the phase term $\Delta\omega_{\mathrm{c}}(t - \nu T_{\mathrm{PR2}})$ is almost constant during the duration of one impulse. Thus, this term has no notable effect on the resulting signal in a properly designed system. Finally, the mixer output $s_{\mathrm{mix}}(t)$ is lowpass-filtered and amplified, yielding

$$s_{\mathrm{out}}(t) = G \cdot \mathrm{LP}\{s_{\mathrm{mix}}(t)\}, \tag{48}$$

where the signal component $s(2\omega_{\mathrm{c}} t)$ is eliminated. The target distance can now be determined by finding the peak in the output signal magnitude, analogous to the radar principle in Section III or the blue sample signal shown in Fig. 5(e).

C. PROPERTIES

With the technique of sequential sampling, the sampling rate and thus, the ADC hardware complexity can be drastically reduced compared to the standard coherent impulse radar. Nevertheless, the LO is still running permanently, even during the unused pulse pause. The power consumption can be further reduced, if the oscillators are only switched on for a very short time. A typical pulse width ranges from 100 ps to 1 ns with a PRF in the range of a few kHz to tens of MHz. Another advantage is the fact that no IQ mixer is required to

Parameter	Value
Frequency	26 GHz
Pulse Width	2 ns
Bandwidth	3 GHz
Range	< 70 m
Accuracy	± 2 mm
P_{Peak}	23.3 mW
P_{avg}	0.076 mW

FIGURE 9. Micropilot FMR51 level gauging radar with a horn antenna from Endress+Hauser AG and its characteristics [31], [32].

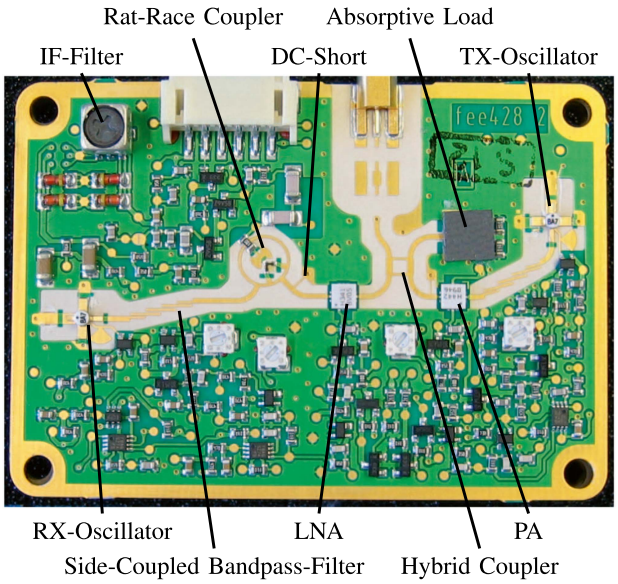

FIGURE 10. RF board of the 26 GHz level radar from Endress+Hauser AG.

demodulate the received signal, which greatly simplifies the hardware complexity and the evaluation of the received signal.

V. APPLICATION EXAMPLES

Sequential sampling radar systems are widely used in different application areas, as the reduced sampling rate simplifies the system design and therefore, reduces the system costs. In the next section, five selected applications are described.

A. LEVEL RADAR

The most widespread industrial application of sequential sampling impulse radars is currently in the field of industrial level measurement. Whereas other systems such as ultrasound or optical systems reach their limits due to extreme temperature and pressure conditions, radar systems stand out because of their great reliability and usability, even when hazardous substances are used. Today, the market offers ready-to-use, integrated impulse radar systems for contactless level measurements of liquids, pastes, sludge, or bulk goods [33], [34].

Endress+Hauser AG, which specializes in measuring devices and solutions for industrial process technology, offers different variants of impulse radar systems to measure the level of liquids with high precision. The first radar systems

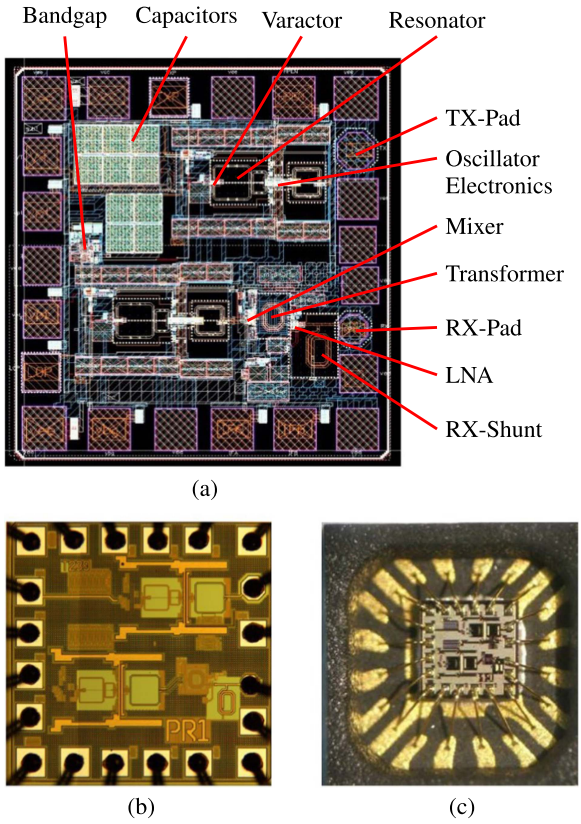

FIGURE 11. Endress+Hauser SiGe BiCMOS pulse radar chip. (a) MMIC chip layout with component labels, (b) bonded MMIC chip with 1.3 mm^2 chip area, and (c) bonded MMIC chip in an open QFN-16 package.

that they introduced to the market in 1993 operated at 6 GHz. Since 2001 products at 26 GHz dominated, as the antenna size was reduced drastically. One example is the free radiating radar system Micropilot FMR51 shown in Fig. 9, which is based on the sequential sampling principle [31] and enables measurements of mm-precision. Micropilot FMR51 utilizes a horn antenna, operates at a frequency of 26 GHz and reaches a precision of ±2 mm. Moreover, it can reliably perform measurements at temperatures in the range of −196 °C to + 450 °C and within a pressure range from vacuum up to 160 bar. The maximum range is 40 m for the standard implementation, but it can be increased to 70 m for the extended version. There are several options for communication, such as the Highway Addressable Remote Transducer (HART) protocol using the traditional 4...20 mA interface or via Bluetooth.

Figure 10 shows the RF-board design of the 26 GHz level radar, using concentrated active and passive components. In contrast to such radar, Fig. 11 shows the pulse radar chip from Endress+Hauser introduced in 2017, which utilizes the monolithic microwave integrated circuit (MMIC) technology to allow mass production and to reduce the physical system size. The integration of central RF components of the radar systems into an MMIC chip enabled the introduction of low-cost radar variants to the market, namely, Micropilot FMR10 [35] and Micropilot FMR20 [36].

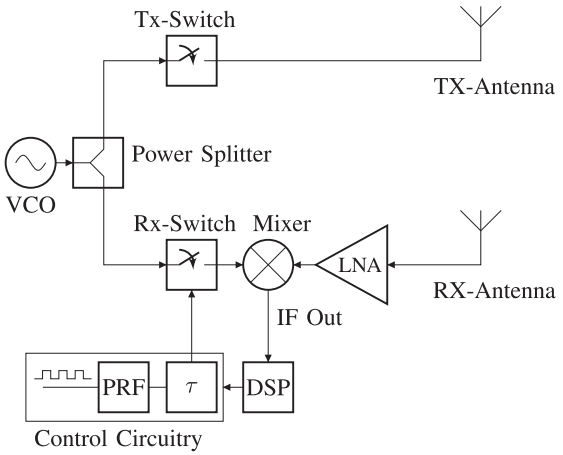

FIGURE 12. Block diagram of the 24 GHz RF frontend of the Tyco M/A-Com radar system [38].

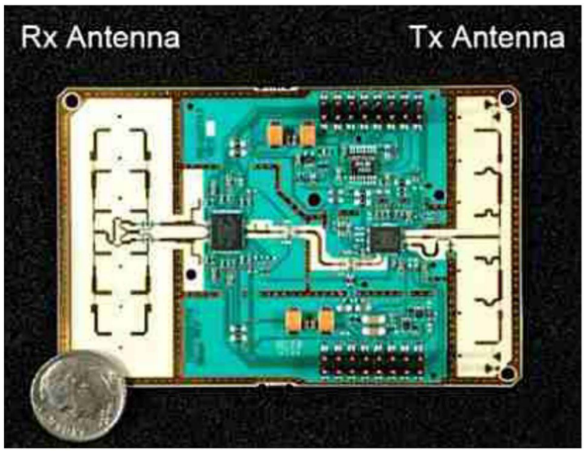

FIGURE 13. Automotive 24 GHz short-range radar system introduced in the Mercedes-Benz S-Class in 2005 [38].

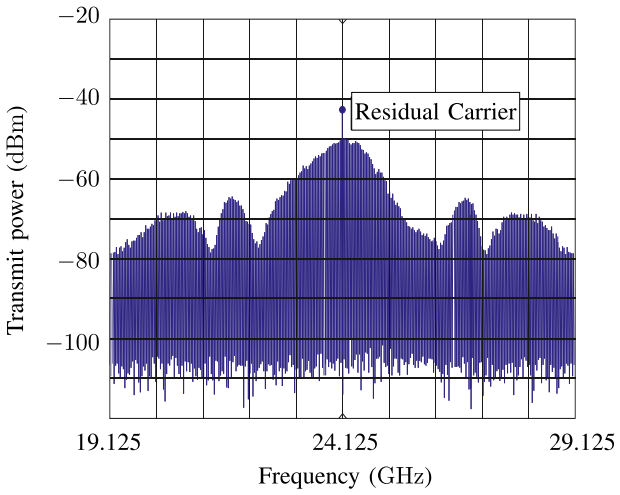

FIGURE 14. Typical transmit spectrum without antenna gain for the automotive short-range radar in Fig. 13.

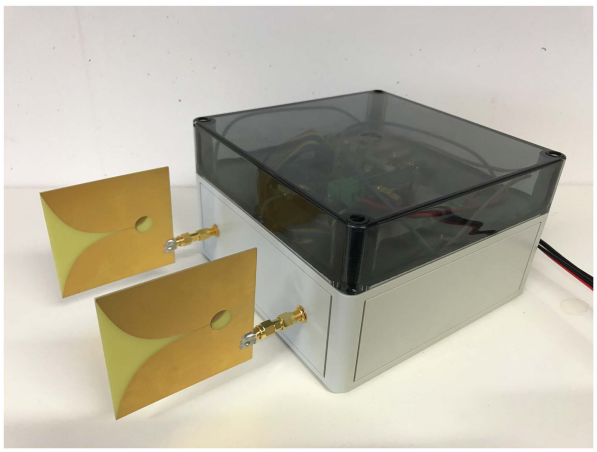

FIGURE 15. Prototype of the sequential sampling impulse radar developed by the authors of this paper. The radar uses two Vivaldi antennas for transmitting and receiving.

Besides the many applications of sequential sampling level gauging radars that have been established on the market for quite a long time, many newly developed systems rely on FMCW radar, such as the 80 GHz Endress+Hauser Micropilot FMR62B [37]. This trend is probably based on the recent advances and the subsequent availability of low-cost radar chips, especially in the higher frequency bands of up to 80 GHz or 120 GHz. It allows for very high bandwidths and hence, extremely precise measurements. The significant advantage of sequential sampling radars, that is, their low power consumption, will remain. Hence, they must not be expected to be completely replaced by FMCW radars, especially at present, with rising energy costs and the focus of companies on reducing their carbon footprint to net-zero.

B. AUTOMOTIVE RADAR

The sequential sampling technique is realized in short-range automotive applications, such as parking aids, blind-spot detection, pre-crash detection, and brake assistants [13], [38].

In 2005, the new Mercedes S-class sedan was equipped with a combination of long-range radar systems and several short-range UWB radar systems to enhance its overall system performance [38]. The short-range radar systems were developed by Tyco M/A-Com and incorporate the sequential sampling principle [13] while operating at 24 GHz with a maximum transmitted power of 17 dBm equivalent isotropic radiated power (EIRP). The block diagram of the radar front end is shown in Fig. 12, with the respective realization displayed in Fig. 13. The radar provides a field of view (FOV) of $\pm 65^\circ$ in azimuth direction and a detection range of up to 30 m. Due to short pulses with pulse widths of approximately 1 n*s*, the radar can achieve a good range resolution in the order of 15 cm. Fig. 14 shows the transmit spectrum of the radar system. As is typical for UWB systems, the very low transmit power spectral density is visible. From 2004 to 2014, around 1.3 million short range radar systems were produced by Tyco M/A-Com.

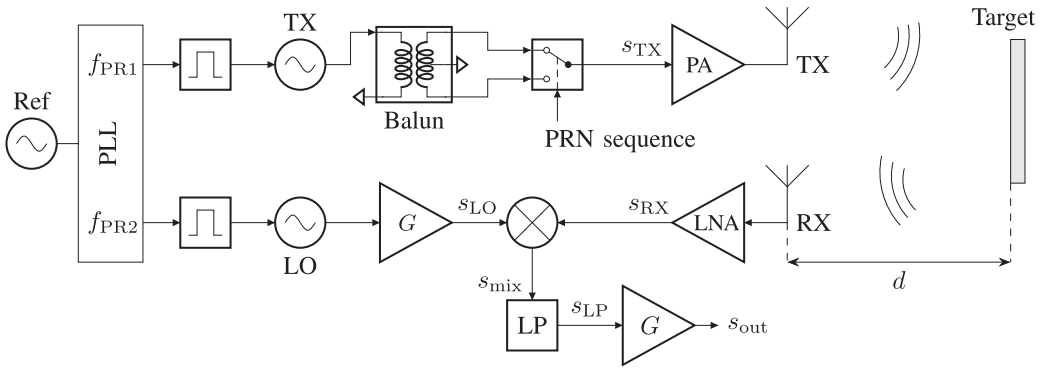

FIGURE 16. Block diagram of the developed radar using sequential sampling combined with PRN sequences. With local oscillator (LO), power amplifier (PA), low noise amplifier (LNA), low pass (LP) filter, analog-to-digital (A/D) converter, amplifier (G), phase-locked loop (PLL), reference clock (Ref), and transmitting (TX) and receiving (RX) antennas.

Furthermore, sequential sampling using switched oscillators has also been used in the pulse oscillator designs in [26], [39]. The goal was to contribute to building a high performance and inexpensive radar system that could possibly replace ultrasound sensors for parking distance control.

However, FMCW radar has replaced the sequential sampling impulse radar in most automotive scenarios because FMCW radar can measure both the range and speed with a high resolution and a better SNR [40], [41]. Examples of switched oscillator sequential sampling radars that are still used for e.g. parking sensors in the automotive world are the A111 and A121 radar chips of Acconeer, which can also be used for level probing or Industry 4.0 applications [42], [43]. The sensors working in the 60 GHz band with very low power consumption show the great potential of the technology even in such higher frequency bands.

C. GROUND PENETRATING RADAR

Besides industrial level sensors and automotive radar applications, radar systems that utilize sequential sampling have been successfully deployed in sounding potash mines to detect stratigraphic features and cracks inside certain layers [44]. The radar system was operating at different frequencies of 100 MHz, 300 MHz, and 600 MHz to address the trade-off between the range resolution and the penetration depth. For higher frequencies, the signal attenuation is usually higher, thus limiting the penetration depth, while for higher signal bandwidths the range resolution is improved [45].

Sequential sampling impulse radar systems have also been used to safely sound icebergs in an airborne configuration, to predict, for example the iceberg drift and its total bulk [46]. The radar system was mounted on a helicopter, with the receiver, transmitter, and antennas positioned 6 m below the helicopter in a net. The radar was operating at a center frequency of 80 MHz and used a pulse width of 20 ns.

Moreover, sequential sampling is exploited in radar systems to analyze and image glacial ice [47], for example, by determining the ice thickness and stratification. In [47], a lightweight and inexpensive radar system was built that consisted of a receiver and a laptop to directly display the measurement results at the test site.

In [48], a sequential sampling impulse radar is integrated into a forefield reconnaissance system (FRS). The FRS is integrated in the top of a melting probe that is designed to melt through thick ice shelves. Besides the radar, the FRS is composed of a sonar system and permittivity sensors, that enables the robust detection of obstacles in the ice. Moreover, the FRS is used to detect the ice–water interface when the melting probe eventually reaches a subglacial reservoir. As the melting speed of the probe is in the order of mh^{-1}, the observed objects are quasi-static, making the sequential sampling technique a reasonable approach.

The radar system of the FRS is currently being developed by the authors of this article using the switched oscillator approach. Fig. 15 shows the first prototype of the radar. Fig. 16 shows the respective block diagram. Both PRFs are derived from a single multi-output phase-locked loop (PLL) chip. Hence, the spreading factor and the PRFs themselves are adjustable to some extent. The PRFs are adjustable in the range of 100 kHz to 1 MHz, which, according to (9), corresponds to an unambigious range of 845 m to 84.5 m in ice. The spreading factor can be set in the range of $\mathrm{SF} = 1,000 \ldots 10,000$. The TX path includes a balun transformer combined with an RF switch for binary phase shift keying (BPSK). This allows the generation of PRN sequences of 180° phase-shifted TX impulses, such as M-sequences, to increase the SNR by up to 42 dB.

The prototype of the radar system uses Vivaldi antennas from [49] for both transmitting and receiving and is shown in Fig. 15. The radar system operates at 1.35 GHz, with a bandwidth of 100 MHz. These result in a range resolution of 0.845 m, assuming a relative permittivity of $\epsilon_r = 3.15$ for ice. Moreover, the output power of the radar prototype is around 20 dBm.

Fig. 17 shows the result of ice radar measurements on the Langenferner glacier in Italy. The right part of the image depicts a reference B-scan, which was recorded with a commercial ground penetrating radar (GPR) that was working at 200 MHz. This B-scan clearly shows the bedrock of the

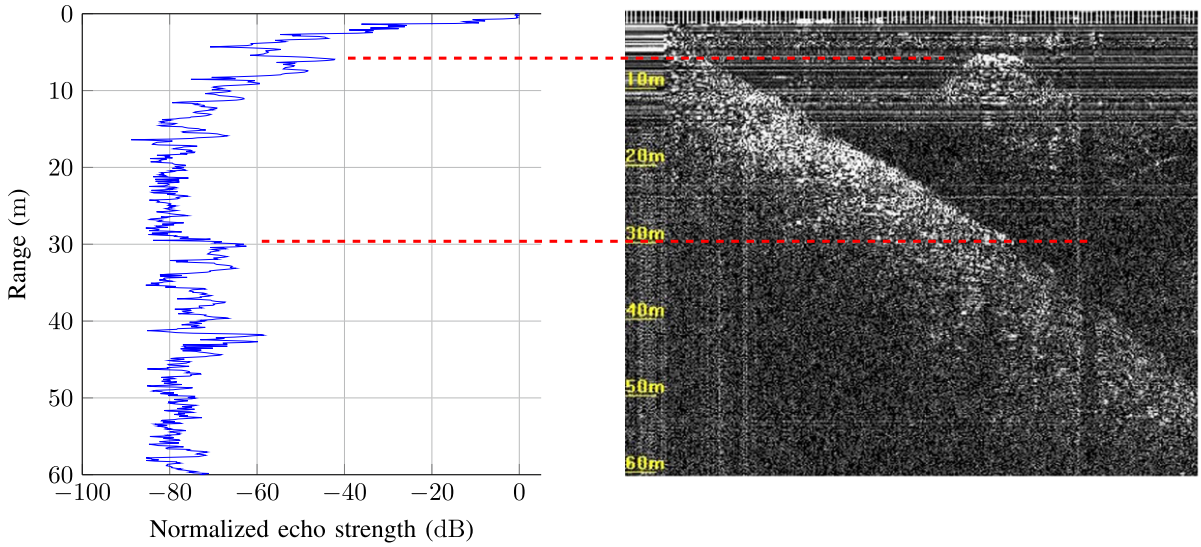

FIGURE 17. Radar measurement on the Langenferner glacier: A-scan at the position of the detected abnormality with the developed radar (left) and the B-scan from a commercial reference system (right).

FIGURE 18. R&SQPS Walk2000 real time walk through security scanner for the detection of items carried on the body [50].

glacier, which starts at around 5 m and steadily increases until an ice thickness of approximately 50 m is reached. Furthermore, there is an anomaly at approximately 6 m, which might be a crevasse. The left side in Fig. 17 shows an A-scan with the radar shown in Fig. 15 at the position on the glacier where the abnormality was detected in the B-scan. The A-scan can confirm the detected abnormality at 6 m, and the bedrock-ice boundary at approximately 30 m.

D. REAL-TIME WALK-THROUGH SECURITY SCANNER

Another novel application of sequential sampling radars is in the field of security scanners. Fig. 18 shows the R&S QPS Walk2000 [50], a non-divesting UWB imaging system that provides three-dimensional information about items carried on the body in realtime, by persons being scanned, who simply walk through the system at a normal pace.

The scanner operates in the frequency range of 3.6 GHz to 10.6 GHz, and therefore, the signal can pass through most clothes. This is why divesting is no longer needed. Furthermore, the system consists of 224 TX modules and 448 RX modules mounted on 28 frontend boards, where only a single TX is active at a time. The maximum mean power spectral density is lower than −41.3 dBm EIRP, according to Part 15 of the Federal Communications Commission (FCC) regulations. The pulse repetition frequency is 12 MHz. The clock is phase-shifted through direct digital synthesis (DDS) in the receiver path to enable the sequential sampling principle with a switched oscillator approach, comparable to the schematic shown in Fig. 8.

The left side of Fig. 19 shows a dummy wearing a jacket with a gun hidden in the left pocket, and the right side shows the corresponding microwave imaging reconstruction. Especially in the left part of the reconstructed image, the gun is clearly visible even through the jacket. Based on the reconstructed images, the hidden items, which can be metallic, ceramic, plastic, liquid, or organic, among others, are automatically detected via artificial intelligence (AI) and are displayed on the avatar as red circles on the screen for the operator. Using the sequential sampling principle, the R&SQPS Walk2000 heralds a new era in terms of real-time, non-divesting security scanners.

E. HUMAN VITAL SIGN DETECTION

Besides the detection of potentially hazardous objects or substances in the vicinity of human bodies, the high bandwidth in the unlicensed 3.1 GHz to 10.6 GHz UWB frequency band provides further opportunities for protecting the safety

TABLE 1. Comparison of the Characteristics of Coherent Impulse Doppler Radar, FMCW Radar, Sequential Sampling Impulse Radar, and Sequential Sampling Impulse Radar With Switched Oscillators

	Coherent impulse Doppler radar	FMCW radar	Sequential sampling impulse radar	Sequential sampling impulse radar with switched oscillators
Power consumption	*high*	*moderate*	*low*	*very low*
RF hardware complexity	*low*	*moderate*	*low*	*very low*
ADC and baseband complexity	*high* (standard), *very high* (with digital impulse compression)	*moderate*	*low*	*very low*
SNR and ranging precision	*poor* (standard), *good* (with impulse compression and/ or averaging)	*very good* (but poor at long range)	*moderate*	*moderate*
Maximum update rate	*high*	*moderate*	*low*	*low*
Velocity measurement/ target tracking	*good*	*very good*	*poor*	*poor*
Range and typical application areas	*long range (medium range)* *military, aerial, or sea surveillance; remote sensing*	*short and medium ranges* *automotive radar, industrial level probing, human gesture/ motion sensing*	*short range (medium range)* *special applications (e.g., ice radar)*	*short range (medium range)* *industrial proximity sensing and level probing, presence detection, special applications*

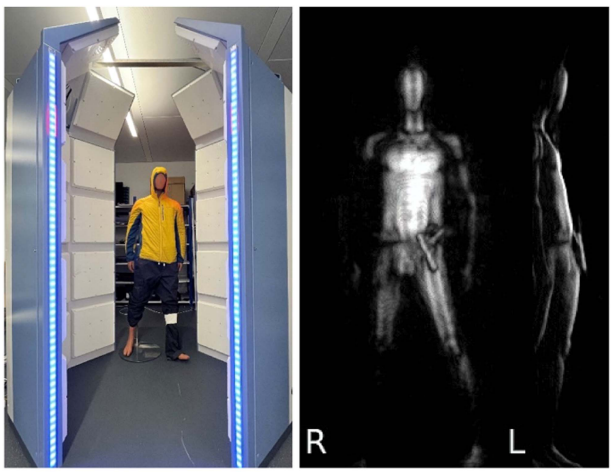

(a) (b)

FIGURE 19. R&SQPS Walk2000 real time walk through security scanner. (a) photograph of the recording situation where a dummy is wearing a jacket with a gun hidden in the left pocket, (b) reconstructed microwave image.

and well-being of humans. Due to these radars' inherently achievable high range resolution and the already mentioned penetration capabilities of UWB systems, they can monitor vital signs of humans, such as breathing or heartbeat [51]. In [52], a UWB radar System-on-Chip (SoC) with an integrated sequential sampling receiver was utilized. From the range-Doppler plots, the motion of the human corpus caused by breathing can be detected. A comparable result, meaning the successful detection of the respiration of females, males, and infants, could be demonstrated by [53] using a switched oscillator approach. Even more impressive is the detection of the human heartbeat, which, unlike breathing, can hardly be seen by other sensor systems, such as cameras. Due to the penetration capability of microwave signals below 10 GHz, they could detect signatures from the heart inside a human chest. Therefore, the pulse rate as well as the heart rate variability was measured with low-cost sequential sampling UWB radar sensors in [54] and [55]. This penetration capability can also be exploited to detect humans and their vital signs behind a wall [56] or to identify anomalies in the wall itself, as with certain commercial wall scanners [57].

VI. COMPARISON

As described in the prior chapters, sequential sampling impulse radar systems are widely used in numerous applications because of certain advantages. In this chapter, these advantages as well as major drawbacks, are compared with other radar types and such comparison is summarized in Table 1. A notable disadvantage of the sequential sampling principle is its comparatively long measurement time and hence, low update rate. In both categories, the standard impulse Doppler radar as well as the FMCW radar outperform the sequential sampling radar. Especially, the FMCW radar has supreme velocity measurement and tracking capabilities, which are why it is often used in highly dynamic applications such as automotive or human motion sensing. Because of the inherent processing gain in an FMCW radar, its SNR is superior to that of coherent impulse Doppler radar systems and sequential sampling radar systems. However, the sequential sampling radar still outperforms the coherent impulse Doppler radar due to the former's correlation receiver. To be fair, a correlation

receiver and averaging can also be utilized in a standard coherent impulse radar, and if the same update rate and the same measurement and averaging times are assumed, the standard impulse radar will always outperform its sequential sampling counterparts due to the noise characteristics illustrated in Section III-III-C of this paper. However, in a standard coherent impulse radar a correlation receiver comes at the cost of increased baseband complexity, which is already comparably high because of the required very high sampling rates. At this point, the main advantages of sequential sampling and especially those of the switched oscillator setup come into play. Besides the low baseband complexity and low ADC sampling rate, the frontend hardware can be quite simple compared to that of a standard FMCW radar. Furthermore, the overall power consumption of a sequential sampling impulse radar is quite low due to the reduced hardware complexity. This is only surpassed by the realization with switched oscillators, as there is no need for a permanently enabled LO. Therefore, the different types of sequential sampling radar systems are often used in short- and partially in medium-range applications such as industrial level probing, which allow for low transmit power and hence- efficient output amplifiers. On the contrary, coherent impulse Doppler radar systems are used in long-range applications such as aerial surveillance, where the comparably high power consumption of hardware does not play a major role compared to extremely high output powers that reach up to several kW or even MW.

VII. CONCLUSION

In this paper, the fundamental theory of the sequential sampling radar principle was described in detail. Furthermore, the sequential sampling radar was compared with other widely used radar principles such as the standard pulse Doppler radar and to the FMCW radar. The sequential sampling radar stands out with its hardware simplicity while achieving a high relative bandwidth especially in the higher frequency domain, low cost, very low power consumption, and high measurement range. The variant with the least cost and the lowest power consumption was achieved by incorporating switched oscillators. Despite the drawbacks of sequential sampling radar, such as their low update rate and velocity measurement and target tracking results compared to other radar principles such as FMCW radar, sequential sampling radar is still a valuable choice for many present-day applications, such as level gauging radar, biomedical radar systems, subsurface inspection and ground penetrating radar, and advanced UWB imaging and personnel security screening systems where moderate update rates are sufficient.

ACKNOWLEDGMENT

The authors thank Winfried Mayer and Dr. Harald Lörch from Endress+Hauser, Hermann Henftling from Veoneer, and the R&S Microwave Imaging Group, particularly Matthias Gareis, for the provided material.

REFERENCES

[1] K. Thurn, R. Ebelt, and M. Vossiek, "Noise in homodyne FMCW radar systems and its effects on ranging precision," in *Proc. IEEE MTT-S Int. Microw. Symp.*, 2013, pp. 1–3.
[2] P. Tschapek, G. Körner, C. Carlowitz, and M. Vossiek, "Detailed analysis and modeling of phase noise and systematic phase distortions in FMCW radar systems," *IEEE J. Microwaves*, vol. 2, no. 4, pp. 648–659, Oct. 2022.
[3] N. Levanon and E. Mozeson, *Radar Signals*. Hoboken, NJ, USA: Wiley, 2004. [Online]. Available: https://onlinelibrary.wiley.com/doi/book/10.1002/0471663085
[4] M. I. Skolnik, "Ground penetrating radar," in *Radar Handbook*. New York, NY, USA: McGraw-Hill, 2008, ch. 21.
[5] M. Unser, "Sampling-50 years after shannon," *Proc. IEEE*, vol. 88, no. 4, pp. 569–587, Apr. 2000.
[6] J. Sachs et al., "Ultra-wideband pseudo-noise sensors and their application in medical engineering, non-destructive testing and for search and rescue," *Inf. Technol. Elect. Eng. - Devices Syst., Mater. Technol. Future*, vol. 54, 2009.
[7] J. Janssen, "An experimental 'stroboscopic' oscilloscope for frequencies up to about 50 MC/S: I fundamentals," *Philips Tech. Rev.*, no. 12, pp. 52–59, 1950.
[8] J. Janssen and A. Michels, "An experimental 'stroboscopic' oscilloscope for frequencies up to about 50 Mc/s: II electrical build-up," *Philips Tech. Rev.*, vol. 12, no. 12, pp. 73–82, 1950.
[9] M. Kahrs, "50 years of RF and microwave sampling," *IEEE Trans. Microw. Theory Techn.*, vol. 51, no. 6, pp. 1787–1805, Jun. 2003.
[10] S. Schuster, S. Scheiblhofer, R. Feger, and A. Stelzer, "Signal model and statistical analysis for the sequential sampling pulse radar technique," in *Proc. IEEE Radar Conf.*, 2008, pp. 1–6.
[11] U. Tietze and C. Schenk, *Halbleiter-Schaltungstechnik*, 12th ed. Berlin/Heidelberg, Germany: Springer, 2002.
[12] A. Leibetseder, C. Wagner, and A. Stelzer, "Concept and realization of an integrated 79-GHz sequential sampling pulse radar," *IEEE Trans. Microw. Theory Techn.*, vol. 67, no. 12, pp. 5372–5383, Dec. 2019.
[13] W. Weidmann and D. Steinbuch, "A high resolution radar for short range automotive applications," in *Proc. 28th Eur. Microw. Conf.*, 1998, pp. 590–594.
[14] S. Hantscher, A. Reisenzahn, H. Kainmüller, and C. G. Diskus, "Hardware concepts for the sequential sampling of repetitive pulse radar echoes in cost-efficient ultra-wideband transceivers," *Microw. Opt. Technol. Lett.*, vol. 52, no. 3, pp. 585–591, 2010.
[15] M. Schartel et al., "Radar-based altitude over ground estimation of UAVs," in *Proc. 11th German Microw. Conf.*, 2018, pp. 103–106.
[16] A. Leibetseder, C. Wagner, and A. Stelzer, "An integrated 79 GHz sequential sampling pulse radar," in *Proc. IEEE MTT-S Int. Microw. Symp.*, 2019, pp. 424–427.
[17] M. Schartel, W. Mayer, and C. Waldschmidt, "Digital true time delay for pulse correlation radars," in *Proc. 13th Eur. Radar Conf.*, Piscataway, NJ, 2016, pp. 330–333.
[18] S.-E. Hamran, "Radar performance of ultra wideband waveforms," in *Radar Technology*, S. Sandoval, Ed. London, UK.: InTechOpen, 2010.
[19] R. Adler, "A study of locking phenomena in oscillators," *Proc. IRE*, vol. 34, no. 6, pp. 351–357, 1946.
[20] B. Razavi, "A study of injection locking and pulling in oscillators," *IEEE J. Solid-State Circuits*, vol. 39, no. 9, pp. 1415–1424, Sep. 2004.
[21] D. Dunwell and A. C. Carusone, "Modeling oscillator injection locking using the phase domain response," *IEEE Trans. Circuits Syst. I, Reg. Papers*, vol. 60, no. 11, pp. 2823–2833, Nov. 2013.
[22] Z. Fan et al., "Injection locking and pulling phenomena in an optoelectronic oscillator," *Opt. Exp.*, vol. 29, no. 3, pp. 4681–4699, 2021.
[23] N. Deparis, A. Boe, C. Loyez, N. Rolland, and P.-A. Rolland, "60 GHz UWB-IR transceiver with pulsed-injected locked oscillator," in *Proc. Eur. Microw. Conf.*, 2007, pp. 1038–1041.
[24] P. Maffezzoni and S. Levantino, "Phase noise of pulse injection-locked oscillators," *IEEE Trans. Circuits Syst. I, Reg. Papers*, vol. 61, no. 10, pp. 2912–2919, Oct. 2014.
[25] A. M. El-Gabaly and C. E. Saavedra, "A 24 GHz quadrature pulsed oscillator for short-range UWB vehicular radar applications," in *Proc. IEEE Int. Symp. Circuits Syst.*, 2011, pp. 1283–1286.
[26] A. Kryshtopin et al., "Cost-minimized 24 GHz pulse oscillator for short-range automotive radar applications," in *Proc. 33rd Eur. Microw. Conf.*, 2003, pp. 1131–1134.

[27] T. Wuchenauer, M. Nalezinski, and W. Menzel, "UWB pulse oscillator at 24 GHz with 2.1 GHz bandwidth for industrial radar sensor applications," in *Proc. IEEE/MTT-S Int. Microw. Symp.*, 2007, pp. 839–842.
[28] D. Kim, D.-W. Kim, and S. Hong, "A 24-GHz power-efficient mmic pulse oscillator for UWB radar applications," *Microw. Opt. Technol. Lett.*, vol. 49, no. 6, pp. 1412–1415, 2007.
[29] A. Leibetseder, C. Wagner, and A. Stelzer, "An integrated coherent startup 79-GHz pulse oscillator for a sequential sampling pulse radar," in *Proc. 15th Eur. Radar Conf.*, 2018, pp. 341–344.
[30] A. Leibetseder, C. Wagner, and A. Stelzer, "A 79 GHz 4RX-2TX SiGe-integrated sequential sampling pulse radar," in *Proc. IEEE MTT-S Int. Conf. Microw. Intell. Mobility*, 2020, pp. 1–4.
[31] Endress Hausser AG, "Technical information micropilot FMR51, FMR52," 2020. [Online]. Available: https://bdih-prod-assetcentralapi-assetcentral-rest-srv.cfapps.eu10.hana.ondemand.com/files/DLA/005056A500261EDAB3AE2266BFE11B4D/TI01040FEN_1020.pdf
[32] J. Roidt and M. Steindl, "Test report no. 20351-08912-7," (edition 3) 2013. [Online]. Available: https://fcc.report/FCC-ID/LCGFMR5XK/2069948.pdf
[33] M. Heim, "Pulse radar for MM-precision in tank gauging," *Hydrocarbon Process.*, no. 80, pp. 65–68, 2001.
[34] J. Motzer, "A pulse radar gauge for level measurement and process control," in *IEEE MTT-S Int. Microw. Symp. Dig.*, 2000, pp. 1563–1566.
[35] Endress Hauser AG, "Technical information micropilot FMR10," 2020. [Online]. Available: https://bdih-prod-assetcentralapi-assetcentral-rest-srv.cfapps.eu10.hana.ondemand.com/files/DLA/005056A500261EEAB8BC9CED11657A12/TI01266FEN_0820.pdf
[36] Endress Hauser AG, "Technical information micropilot FMR20," 2020. [Online]. Available: https://bdih-prod-assetcentralapi-assetcentral-rest-srv.cfapps.eu10.hana.ondemand.com/files/DLA/005056A500261EEAB8BCB76D61B25AA9/TI01267FEN_0820.pdf
[37] Endress Hauser AG, "Technical information micropilot fmr60b hart," 2022. [Online]. Available: https://bdih-download.endress.com/files/DLA/005056A500261EDD81D463EC6DD3AED2/TI01683FEN_0122-00.pdf
[38] J. Wenger, "Short range radar - Being on the market," in *Proc. Eur. Microw. Conf.*, 2007, pp. 1534–1537.
[39] A. Leibetseder and A. Stelzer, "Doppler effect in a 79-GHz sequential sampling pulse radar," in *Proc. 18th Eur. Radar Conf.*, 2022, pp. 329–332.
[40] S. M. Patole, M. Torlak, D. Wang, and M. Ali, "Automotive radars: A review of signal processing techniques," *IEEE Signal Process. Mag.*, no. 34, no. 2, pp. 22–35, Mar. 2017.
[41] C. Waldschmidt, J. Hasch, and W. Menzel, "Automotive radar – From first efforts to future systems," *IEEE J. Microwaves*, vol. 1, no. 1, pp. 135–148, Jan. 2021.
[42] Acconeer AB, "Xm132 entry module datasheet," Malmö, 2022. [Online]. Available: https://developer.acconeer.com/download/xm132-datasheet-pdf/
[43] M. Ärlelid, D. Chouvaev, and M. Egard, "Transmitter-receiver system," U.S Patent 2018164419A1, Jun. 6, 2018.
[44] A. P. Annan, J. L. Davis, and D. Gendzwill, "Radar sounding in potash mines, saskatchewan, Canada," *Geophysics*, vol. 53, no. 12, pp. 1556–1564, 1988.
[45] D. J. Daniels, *Ground Penetrating Radar* (IEE Radar, Sonar, Navigation and Avionics Series), vol. 15, 2nd ed. London, U.K.: Inst. Elect. Engineers, 2007.
[46] J. R. Rossiter and K. A. Gustajtis, "Iceberg sounding by impulse radar," *Nature*, vol. 271, no. 5640, pp. 48–50, 1978.
[47] F. Jones, B. B. Narod, and G. Clarke, "Design and operation of a portable, digital impulse radar," *J. Glaciol.*, vol. 35, no. 119, pp. 143–148, 1989.
[48] D. Heinen et al., "The TRIPLE melting probe - An electro-thermal drill with a forefield reconnaissance system to access subglacial lakes and oceans," in *Proc. OCEANS*, San Diego - Porto, 2021, pp. 1–7.
[49] M. Stelzig et al., "Virtual synthetic aperture radar target based on a miniaturized monostatic digital delay transponder," *IEEE Microw. Wireless Compon. Lett.*, vol. 32, no. 3, pp. 249–252, Mar. 2022.
[50] Rohde & Schwarz GmbH & Co KG, " R&SQPS Walk2000 security scanner," 2022. [Online]. Available: https://scdn.rohde-schwarz.com/ur/pws/dl_downloads/dl_common_library/dl_brochures_and_datasheets/pdf_1/QPS_Walk2000_fly_en_3608-1946-32_v0400.pdf
[51] D. T. Wisland, K. Granhaug, J. R. Pleym, N. Andersen, S. Stoa, and H. A. Hjortland, "Remote monitoring of vital signs using a CMOS UWB radar transceiver," in *Proc. 14th IEEE Int. New Circuits Syst. Conf.*, Piscataway, NJ, 2016, pp. 1–4.
[52] D. Zito et al., "SoC CMOS UWB pulse radar sensor for contactless respiratory rate monitoring," *IEEE Trans. Biomed. Circuits Syst.*, vol. 5, no. 6, pp. 503–510, Dec. 2011.
[53] B. Schleicher, I. Nasr, A. Trasser, and H. Schumacher, "IR-UWB radar demonstrator for ultra-fine movement detection and vital-sign monitoring," *IEEE Trans. Microw. Theory Techn.*, vol. 61, no. 5, pp. 2076–2085, May 2013.
[54] M. Mahler, H.-O. Ruob, and W. Menzel, "Radar sensors to determine position and physiological parameters of a person in a vehicle," in *Proc. 32nd Eur. Microw. Conf.*, 2002, pp. 1–4.
[55] I. Y. Immoreev, S. Samkov, and T.-H. Tao, "Short-distance ultra wideband radars," *IEEE Aerosp. Electron. Syst. Mag.*, vol. 20, no. 6, pp. 9–14, Jun. 2005.
[56] Z. Zhengliang, Y. Degui, Z. Junchao, and T. Feng, "Dataset of human motion status using IR-UWB through-wall radar," *J. Syst. Eng. Electron.*, vol. 32, no. 5, pp. 1083–1096, 2021.
[57] Robert Bosch Tool Corporation, "Safety instructions wallscanner D-tect TM150," 2009. [Online]. Available: https://www.manualslib.com/manual/1552074/Bosch-Wallscanner-D-Tect-150.html#manual

MARTIN VOSSIEK (Fellow, IEEE) received the Ph.D. degree from Ruhr-Universität Bochum, Bochum, Germany, in 1996. In 1996, he joined Siemens Corporate Technology, Munich, Germany, where he was the Head of the Microwave Systems Group, from 2000 to 2003. Since 2003, he has been a Full Professor with Clausthal University, Clausthal-Zellerfeld, Germany. Since 2011, he has been the Chair of the Institute of Microwaves and Photonics (LHFT), Friedrich-Alexander-Universität Erlangen-Nürnberg (FAU), Erlangen, Germany. He has authored or coauthored more than 350 articles. His research has led to more than 100 granted patents. His research interests include radar, microwave systems, wave-based imaging, transponder, RF identification, communication, and wireless locating systems. He is a member of the German National Academy of Science and Engineering (acatech) and of the German research foundation (DFG) review board. He is a member of the IEEE Microwave Theory and Technology (MTT) Technical Committees MTT-24 Microwave/mm-wave Radar, Sensing, and Array Systems, MTT-27 Connected and Autonomous Systems (as Founding Chair), MTT-29 Microwave Aerospace Systems. He is also serving on the advisory board of the IEEE CRFID Technical Committee on Motion Capture & Localization. He was the recipient of numerous best paper prices and other awards. In 2019, he was awarded with the Microwave Application Award from the IEEE MTT Society (MTT-S) for Pioneering Research in Wireless Local Positioning Systems. Dr. Vossiek has been a member of organizing committees and technical program committees for many international conferences and he has served on Review Boards for numerous technical journals. From 2013 to 2019, he was an Associate Editor for IEEE TRANSACTIONS ON MICROWAVE THEORY AND TECHNIQUES. Since October 2022, he has been an Associate Editor-in-Chief for IEEE TRANSACTIONS ON RADAR SYSTEMS.

NIKLAS HABERBERGER was born in Karlstadt, Germany, in 1995. He received the M.Sc. degree in electrical engineering from Friedrich-Alexander-Universität Erlangen-Nürnberg (FAU), Erlangen, Germany, in 2020, where he is currently pursuing the Ph.D. degree. In 2020, he joined the Institute of Microwaves and Photonics of FAU. His research interests include radar hardware design, signal processing, and system design.

LENA KRABBE (Student Member, IEEE) was born in Bergisch-Gladbach, Germany, in 1995. She received the M.Sc. degree in electrical engineering from Friedrich-Alexander-Universität Erlangen-Nürnberg (FAU), Erlangen, Germany, in 2022, where she is currently working toward the Ph.D. degree. In 2022, she joined the Institute of Microwaves and Photonics of FAU. Her research interests include radar algorithms and concepts in the application of ice radar and glaciology.

MARKUS HEHN (Member, IEEE) was born in Bamberg, Germany, in 1987. He received the M.Sc. and Ph.D. degrees from Friedrich-Alexander-Universität Erlangen-Nürnberg (FAU), Erlangen, Germany, in 2016 and 2021, respectively. He is currently a Postdoc Researcher with the Institute of Microwaves and Photonics, FAU. His research interests include radar for near-field localization and localization systems for indoor environment.

CHRISTIAN CARLOWITZ (Member, IEEE) received the Dipl.-Ing. degree in information technology from the Clausthal University of Technology, Clausthal-Zellerfeld, Germany, in 2010, and the Dr.-Ing. degree from the Friedrich-Alexander-Universität Erlangen-Nürnberg (FAU), Erlangen, Germany, for his thesis on wireless high-speed communication based on regenerative sampling. He is currently with the Institute of Microwaves and Photonics, FAU, where he has been leading the Microwave and Photonic Systems Group since 2018. His research interests include conception, design, and implementation of innovative system architectures for radar and communication frontends at microwave, mm-wave, and optical frequencies. He focuses especially on hardware concepts, and analog and digital signal processing techniques, for ultra-wideband high-speed communication systems, full-duplex mobile communication transceivers, and massive MIMO base stations, and also for ranging and communication with mm-wave RFID systems. Dr. Carlowitz is a member of the IEEE Microwave Theory and Techniques Society, the IEEE MTT-S Technical Committee RF/Mixed-Signal Integrated Circuits and Signal Processing (MTT-15), and the International Microwave Symposium Technical Program Review Committee. He is a regular reviewer for IEEE TRANSACTIONS ON MICROWAVE THEORY AND TECHNIQUES and several additional international conferences, including EuMW and ICMIM.

MICHAEL STELZIG was born in Munich, Germany, in 1993. He received the M.Sc. degree in mechatronics from Friedrich-Alexander-Universität Erlangen-Nürnberg (FAU), Erlangen, Germany, in 2018, where he is currently working toward the Ph.D. degree. In 2018, he joined the Institute of Microwaves and Photonics of FAU. His research interests include radar systems and signal processing in the context of glacial exploration.